Università Cattolica del Sacro Cuore

Sede di Brescia

Facoltà di Scienze Matematiche, Fisiche e Naturali

Corso di Laurea di Primo Livello in Fisica

Second Harmonic Generation with ultra-short laser pulses in KNS ceramic glasses

Relatore:

Ch.mo Dott. Gabriele Ferrini

Correlatore:

Ch.mo Dott. Claudio Giannetti

Laureando: **Luca Bignardi**

mat. 3203143

Anno Accademico 2005/2006

Contents

Introduction

Optical frequency converters are widely used to generate coherent light at frequencies at which laser light is unavailable. Standard devices can have a very high efficiency, but they are usually based on pure, and hence expensive, nonlinear single crystals that also require careful adjustments.

Recent works demonstrated that pure, perfectly regular crystals are not essential for the efficient operation of nonlinear optical devices [1]. Now it seems that polycrystalline materials might be interesting second harmonic converter, even if with conversion efficiency lower than a standard nonlinear crystalline converter.

For example, the potassium niobium silicate ceramic glasses (KNS) are policrystalline transparent materials that show the second harmonic generation property, probably due to the inhomogeneity at the nanoscale. These glasses have no ordered structure. They consist of a glassy matrix, where nano-crystalline elements are disposed in a totally random way.

Different kinds of glasses may be obtained changing the percent quantities of potassium (K), niobium (N) and silicon (S) in the preparation process.

The size of nanocrystals can be controlled varying the duration of annealing process, i.e. a secondary thermal treatment just above the glassification temperature. [6, 7, 11]

Our aim is the analysis of KNS optical proprieties upon excitation with IR pulsed laser light. We want to quantitatively estimate the second harmonic generation (SHG) in five samples, different in composition and preparation process.

In particular, we have proved that the SH was due to bulk effects. This feature indeed is not peculiar of polycrystalline elements, where the SHG is prohibited by symmetry conditions.

Finally we've examined the difference in SH conversion efficiency between annealed glasses and glasses not subject to this thermal process. Our aim was to determine if the annealing process increases the KNS glasses SHG efficiency.

1. Characterization of samples

For our work, we analyzed samples prepared by the staff of the Department of Materials and Production Engineering at the University of Naples.[6]

1.1 Harmonics generation in polycrystalline materials

In the last ten years, several works described amorphous or nano-crystallized ceramic glasses showing a second harmonic generation (SHG) behavior (see [12, 13, 14, 15, 16, 17]).

The potassium niobium silicate ceramic glasses (KNS) are polycrystalline materials in which the second harmonic generation process was observed. The polycrystalline nature of the materials was revealed with a x-ray diffraction analysis [6, 7]. The SHG seems to be due to the nanocrystals that compose the material and related to their dimensions. Hence the material, at nanoscale, is not homogeneous.

At the present state, a physical model that allows the interpretation of

second harmonic generation (SHG) in KNS glasses is not available[1]. In particular, it's not trivial to write down the polarization vector for this kind of materials, because they are macroscopically polycrystalline and we do not know the form of dielectric tensor.

However, it should be emphasized that the SHG effect in glasses has exclusively electric-induced nature and does not involve noticeable atomic rearrangements on the scale of both short-range and medium-range orders.

1.2 **Production of samples**

The samples we have studied are potassium niobium silicate ceramic transparent ceramic glasses. They are composed by potassium niobium silicate nanocrystals precipitate on a glassy matrix. Each sample is identified with the percent composition of K_2O, Nb_2O_5 and SiO_2, the duration and temperature of annealing process.

Sample	K(%)	Nb(%)	Si(%)	annealing period	annealing T(°C)
S1	23	27	50	2h	680
S2	20	25	55	2h	705
S3	23	27	50	10h	680
S4	20	25	55	10h	705
S5	30	30	40	2h	650

Glasses, whose composition is reported in table, were obtained melting KNO_3, Nb_2O_5 and SiO_2 in a platinum crucible at T=1500°C for 1h. Then, the melted was deposed on a brass plate warmed at T=300°. Eventually the

[1] A first tentative of explain this phenomenon was made in [3] and [7]

glass was annealed a temperature close to glass-solidification temperature T_g. The value of the T_g temperature was obtained with a differential thermal analysis (DTA) process.

This second thermal process causes the growth of nanocrystal in the glass matrix. The crystallization of glasses occurs with two process: the nucleation and the crystal growth. These processes occur only above T_g. The nucleation speed is greater at T_g while the maximum of the crystallization growth speed is above T_g.

So the samples, that are nanocrystalline glasses, was obtained maximizing the crystalline nuclei number growth with respect to the crystalline growth. Hence, the annealing process at T_g allows us to obtain a material with a lot of crystals with slow growth.

We also have analyzed as-quenched glasses, i.e. they have not received the annealing process we've just described. The role of annealing process will be clearer in the measurements chapter.

1.3 **Linear Lorentz Oscillator**

We give only some basic elements concerning the process of second-harmonic generation in nonconducting media. Thus our exposal will not use the quantum theory of nonlinear optics. We will present a classical model but very useful in order to explain the basic concept of nonlinear optics.

A very simple and intuitive model to explain the interaction of electromagnetic waves with matter is the Lorentz oscillator. Although it is a classical-electrodynamics based model, it gives reason of a great numbers of phenomena, such as the polarization of dielectric linear media.

We study a dielectric isotropic medium interacting with an external, sinusoidal, electric field of an electromagnetic wave:

$$E(t) = E_0 \cos(\omega t)$$

The behavior of the bound electron can be seen as the motion of a classical damped oscillator driven by an external drive force with frequency ω. The effects due to the magnetic field of the electromagnetic wave are negligible.

In general, the electrons are bound to the atoms with forces whose description can be very difficult. However, assuming that the potential depends only on the position, we can expand the potential associated to bound forces in Taylor series around the stable equilibrium position $x = 0$:

$$V(x) = V(0) + \left.\frac{\partial V(x)}{\partial x}\right|_0 x + \frac{1}{2}\left.\frac{\partial^2 V(x)}{\partial x^2}\right|_0 x^2 + \cdots = \sum_{n=0}^{\infty}\left[\left.\frac{\partial^n}{\partial x^n}V(x)\right|_0 \frac{x^n}{n!}\right] \quad (1.1)$$

For the first two terms of the expansion we have :

$$V(0) = const. \quad \text{(the constant is arbitrary, we choose } const = 0)$$

$$\left.\frac{\partial}{\partial x}V(x)\right|_{x=0} = 0 \qquad \text{(x=0 is an equilibrium position)}$$

Because $x = 0$ is a minimum for the potential, the quadratic term of the potential is positive. So we can use the little oscillations approximation. The damping is due to oscillating dipole radiation. The charge oscillates under the action of the external field and so it irradiates.

The motion equation for a single charge (in a one-dimensioned space) is composed by the following terms:

$$m\ddot{\mathbf{x}} = \mathbf{F}_{binding} + \mathbf{F}_{damping} + \mathbf{F}_{driving}. \quad (1.2)$$

that is

$$m\ddot{\mathbf{x}} = -\frac{\partial V(x)}{\partial x} + m\gamma\dot{x} + \mathbf{F}_{driving}, \tag{1.3}$$

If we insert the potential written in (1.1), we obtain the equation for the motion of the electron:

$$\ddot{x} + \gamma\dot{x} + \sum_{n=2}^{\infty} \frac{\partial^n V(x)}{\partial x^n}\bigg|_0 \frac{x^{n-1}}{(n-1)!} = \frac{qE}{m}\cos\omega t \tag{1.4}$$

If we expand only to $n = 2$, we will obtain the equation of an harmonic linear oscillator, that is:

$$\ddot{x} + \gamma\dot{x} + \omega_0^2 x = \frac{q}{m}E_0\cos(\omega t) \tag{1.5}$$

This is the real part of the complex equation:

$$\tilde{\ddot{x}} + \gamma\tilde{\dot{x}} + \omega_0^2\tilde{x} = \frac{q}{m}\tilde{E}_0\, e^{-i\omega t}. \tag{1.6}$$

Because the driving force is sinusoidal with frequency ω, a solution for this differential equation will be an oscillating solution with frequency ω:

$$\tilde{x}(t) = x_0(\omega)e^{-i\omega t}.$$

The $x_0(\omega)$ are the coefficient of Fourier expansion in ω of $x(t)$, that is:

$$x_0 = \frac{q/m}{\omega_0^2 - \omega - i\gamma\omega}E_0,$$

where ω_0 is the proper frequency of the oscillator.

In this case the charge emits only at ω, because we have supposed a particular condition on the potential. The dipole moment of the single electron $\mathbf{p}$ is the real part of:

$$\tilde{p}(t) = q\tilde{x}(t) = \frac{q^2/m}{\omega_0^2 - \omega - i\gamma\omega}E_0 e^{-i\omega t}.$$

1.4 Polarization vector

A peculiar feature of isotropic media is that we can write the polarization vector as

$$\mathbf{P} = nq\mathbf{x} = \frac{nq^2/m}{\omega_0^2 - \omega^2 - i\gamma\omega}\mathbf{E},$$

where $n = \frac{N}{V}$ is the number of electrons in volume unit. The coefficient relating the polarization vector $\mathbf{P}$ to the external field $\mathbf{E}$ is a scalar value χ (electrical susceptibility).

But, in a more general situation (such as in crystals), the polarization induced by a wave in the matter can depend on the direction of propagation of the wave. Thus in non-isotropic media, the force that binds electrons is different along different direction of the medium. Therefore the dependence of $\mathbf{P}$ from $\mathbf{E}$ is expressible only by the $\hat{\chi}$ susceptibility tensor:

$$P_i = \epsilon_0 \chi_{ij} E_j, \tag{1.7}$$

or in matrix notation

$$\begin{pmatrix} P_x \\ P_y \\ P_z \end{pmatrix} = \epsilon_0 \begin{pmatrix} \chi_{11} & \chi_{12} & \chi_{13} \\ \chi_{21} & \chi_{22} & \chi_{23} \\ \chi_{31} & \chi_{32} & \chi_{33} \end{pmatrix} \begin{pmatrix} E_x \\ E_y \\ E_z \end{pmatrix} \tag{1.8}$$

For ordinary non-absorbing crystals, this tensor is symmetric and we can define a set of principal axes. In such a way the tensor becomes diagonal:

$$\hat{\chi} = \begin{pmatrix} \chi_{11} & 0 & 0 \\ 0 & \chi_{22} & 0 \\ 0 & 0 & \chi_{33} \end{pmatrix}.$$

1.5 **Nonlinear perturbative approach**

We are interested now to explore the case of more general potential, always in nonconducting isotropic media. Therefore we shall consider the nonlinear terms in the expansion (1.1) that will produce harmonics of ω.

If in equation (1.1) we continue the expansion up to term $n = 3$, we obtain a cubic term for the potential. In such a situation, we are dealing with nonlinear effects because we have a quadratic term for the force.

We solve the nonlinear equation, supposing that nonlinear effects introduce a small perturbation in linear Lorentz oscillator (1.3).

We can write the position x as series of harmonics of the driven frequency ω,

$$x = X_1 \cos(\omega t + \phi_1) + X_2 \cos(2\omega t + \phi_2) + X_3 \cos(3\omega t + \phi_3) + \cdots$$

or, in complex notation

$$\tilde{x} = \frac{X_1}{2}(e^{i\omega t} + e^{-i\omega t}) + \frac{X_2}{2}(e^{2i\omega t} + e^{-2i\omega t}) + \frac{X_3}{2}(e^{3i\omega t} + e^{-3i\omega t}) + \cdots$$

with $X_1 \gg X_2 \gg X_3, \cdots$, for the consistence of perturbation approach.

After substitution in (1.4), we obtain linear and nonlinear terms in ω, 2ω. We are interested to derive X_1 and X_2 (they will be useful for deriving the polarization vector):

$$X_1 = \frac{qE_0}{m}\frac{1}{D(\omega)} \tag{1.9}$$

$$X_2 = -\frac{1}{2 \cdot 2!}\frac{\partial^3 V(x)}{\partial x^3}\bigg|_0 \left(\frac{qE_0}{m}\right)^2 \frac{1}{D(\omega)^2 D(2\omega)}, \tag{1.10}$$

with $D(\omega) = \omega_0^2 - \omega^2 - i\gamma\omega$.

We know the polarization vector $\mathbf{P}$ induced by the field $E(t) = E_0 e^{-i\omega t}$, in a isotropic medium. Now we expand this vector around E=0 as:

$$\mathbf{P} = \epsilon_0 \chi \mathbf{E}(t) \simeq \epsilon_0 (\chi^{(1)} E_0 e^{-i\omega t} + \chi^{(2)} E_0 e^{-2i\omega t} + \cdots) \tag{1.11}$$

But another expression for $\mathbf{P}$ is known, derived from

$$\mathbf{P} = nq\mathbf{x} \simeq nqX_1 e^{-i\omega t} + nqX_2 e^{-2i\omega t} + \cdots = \frac{nq^2 E_0}{mD(\omega)} e^{-i\omega t} - \frac{nq^3}{2}\left(\frac{E_0}{m}\right)^2 \frac{1}{D(\omega)^2 D(2\omega)} \frac{1}{2!} \frac{\partial^3 V}{\partial x^3}\bigg|_0 e^{-2i\omega t} + \cdots \tag{1.12}$$

Equating the two previous expressions, we obtain the values for $\chi^{(1)}$ and $\chi^{(2)}$ as function of the incident field $\mathbf{E}$:

$$\chi^{(1)} = \frac{nq^2}{\epsilon_0 m\, D(\omega)} \qquad \chi^{(2)} = -\frac{nq^3}{2\epsilon_0 m^2} \frac{1}{D(\omega)^2 D(2\omega)}. \tag{1.13}$$

Notice that by assumption, the external field must be small with respect to the field E_{at} that binds the electron to its atom, otherwise we can't use the perturbative method and consequently expand χ in series.

In case of crystalline media, we are no free charges so the divergence of the displacement vector $\mathbf{D}$ is zero. The expansion (1.11) hence becomes:

$$P_i = \epsilon_0 (\chi_{ij} E_j + \chi^{(2)}_{ijk} E_j E_k + \cdots) \tag{1.14}$$

where χ_{ij} is an element of the ordinary susceptibility tensor. $\chi^{(2)}_{ijk}$ represents an element of a third order tensor.

We can separate the polarization as sum of linear and nonlinear terms. The nonlinear term is

$$P_i^{NL} = \epsilon_0 \chi^{(2)}_{ijk} E_j E_k + o(\mathbf{E}^3) \cdots \tag{1.15}$$

1.6 Second harmonic generation in crystals

The first term of (1.15) equation corresponds to a variation at twice the fundamental frequency. This process is known as second harmonic generation (SHG).

Notice that in a isotropic centrosymmetrical material (that has an inversion symmetry), **P** is an odd function.

Thus, the application of the inversion operator $\mathfrak{I}$ to polarization vector **P** gives:

$$\mathfrak{I}(P_i) = \mathfrak{I}(\chi^{(2)}_{ijk} E_j E_k)$$

$$-P_i = \chi^{(2)}_{ijk}(-E_j)(-E_k). \tag{1.16}$$

But a sign reversal of P_i gives:

$$-P_i = -\chi^{(2)}_{ijk} E_j E_k, \tag{1.17}$$

due to the vectorial nature of the polarization **P**. So the conditions expressed in equation 1.16 and 1.17, cause the vanishing of the $\chi^{(2)}$ tensor.

This fact may be also explicated saying that an inversion symmetry of the potential produces the vanishing of all odd derivatives of the potential in the equilibrium position. In particular, if the third derivative of V(x) vanishes, we have no SHG effects.

Therefore, the SHG process is not allowed in centrosymmetric or amorphous material, but only in materials with asymmetric charge distribution, such as piezoelectric crystals.

However, it is possible produce SH at surfaces of an amorphous material, because surfaces are the unique zone of an amorphous material where there is a lack of inversion symmetry[10].

Now suppose we have a slab of thickness l of a noncentrosymmetrical crystal. Suppose we have an incoming wave $E_\omega e^{i(k_\omega z-\omega t)}$ with a frequency ω, that propagate in z direction. This wave induces in the medium a polarization vector that has a linear and a quadratic term, such as in (1.14). So, the nonlinear polarization of medium causes the reradiation of the electrons energy at doubled frequency.

The out-coming second harmonic $E_{2\omega}e^{i(k_{2\omega}z-2\omega t)}$ has an amplitude proportional to the square of the incoming electrical field, integrated upon all the contributions of each element of thickness dz in the crystal, namely:

$$E(2\omega, l) \propto \int_0^l E^2(\omega, z)\, \mathbf{d}z \propto \int_0^l e^{2i[k_\omega z-\omega(t-\tau)]}\, \mathbf{d}z. \tag{1.18}$$

By solving the integral and taking the square absolute value, we find the intensity of SH:

$$I_{2\omega} \propto \left[\frac{\sin(k_\omega - \frac{1}{2}k_{2\omega})l}{k_\omega - \frac{1}{2}k_{2\omega}}\right]^2 \tag{1.19}$$

This yields the result that $I_{2\omega}$ has its maximum when $k_\omega = \frac{1}{2}k_{2\omega}$.

If $\Delta k \neq 0$, the second harmonic generated in some plane z_1 is not in phase with the SH generated at z_2. This results in the interference described by factor given in (1.19). The spatial distance corresponding to 2π dephasing between two z planes is called *coherence length* Λ_c

$$\Lambda_c = \frac{2\pi}{2k_\omega - k_{2\omega}},$$

that is the maximum crystal length that is useful to produce SH intensity.

The maximum of $I_{2\omega}$ is obtained when the phase velocity of the fundamental wave equals to the phase velocity of the wave at doubled frequency. This condition is named *phase-matching*.

If we use the relation $k_\omega = \omega\sqrt{\mu\epsilon_0}n_\omega$, we obtain $n_\omega = n_{2\omega}$. So, to have phase-matching condition, the indices of refraction (and then the phase velocity) of the fundamental and of the second harmonic must be equal. Therefore it is impossible to satisfy the phase-matching condition using a material with a normal dispersion law because the phase velocity depends on the frequency.

The technique that is used to satisfy the $\Delta k = 0$ condition takes advantage of the natural birefringence of anisotropic crystals.

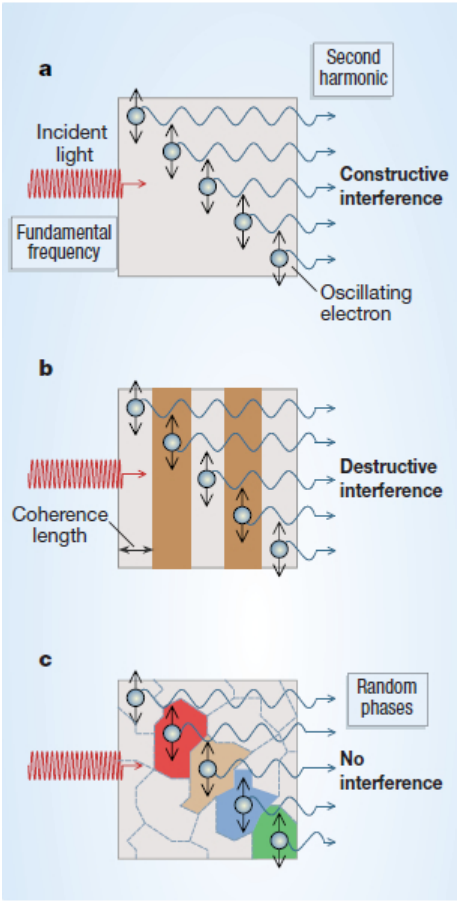

Figure 1.1: The SHG in different kinds of optical materials [2]

Thus, in order to obtain phase-matching, a birefringent crystal has to be

used, in which the polarization of incident light and its direction influences the speed of propagating waves. By a suitable choice of incidence angle of the fundamental, the second harmonic waves generated by the planes in crystal interfere constructively (situation (a) figure 1.1).

This allows to increase the second harmonic produced of several orders of magnitude.

The intensity of SH depends on critically by the intensity of the incoming radiation. In order to see an appreciable SH signal we have to use a continuous radiation with an high power.

An alternative method is using pulsed radiation, with a low mean power but high pulse intensity. In such a way, the second harmonic conversion efficiency $I_{2\omega}$ is greater than using a continuous light source.

In order to obtain crystalline SH generators, we have to grow the crystal layer by layer and cut a thin slab, compatible with the phase-matching conditions, with an expensive process.

In last years, some works demonstrated that such of a nonlinear crystal is not necessary in order to produce SH [1, 2]. Now it seems that a competitive alternative to the traditional approach might indeed be provided by the random quasi-phase-matching (situation (c) figure 1.1).

We can use a polycrystalline disordered sample, consisting of a large number of single-crystal domains with random orientations, random shapes and random sizes. The frequency-converted waves generated by different domains – be they second harmonic waves, as in our example – achieve random phases and interfere neither constructively nor destructively.

The total intensity of the generated wave is then the sum of the intensities

arising from individual domains and it grows linearly with the number of domains or the length of the sample.

Clearly the random phase-matching is less efficient than the usual phase-matched process but it outperforms the phase-mismatched process for which the interference of partial waves is destructive. Random quasi-phase-matching does not require the growth of large single crystals, and needs neither a careful alignment of the optical setup nor the high precision engineering of microstructured samples.

The new technique is well suited to isotropic semiconductors (such as ZnSe, GaAs and GaP), which are technologically important and industrially mature materials.

KNS samples are very similar to the glasses presented in [2]. Macroscopically, the KNS are glasses, i.e. they are amorphous and without a defined crystalline lattice. However, a x-ray analysis revealed that KNS are nanostructured, and these crystals evidenced SHG properties.

We have seen that KNS, generates SH in the bulk of the material and not at surfaces.

The SHG process seems to be due to a random quasi-phase-matching condition, where distinct single nano-crystal domains generate waves with random phases, precluding any destructive interference effects. The resulting intensity is the sum of intensities due to individual domains and hence grows linearly with the number of domains in the length of the sample.

Clearly the SHG efficiency is very smaller than in case of a single nonlinear phase-matched crystal. However KNS are interesting because they avoid the preparation of refined nonlinear crystalline elements, in order to satisfy the

phase-matching condition.

We want to examine in a quantitative way, the efficiency of SHG in KNS and compare it with the efficiency of a BBO crystal. We will prove that the SHG is a bulk effect that probably involves the crystalline structure at the nanoscale.

2. Experimental set-up

We have performed three kinds of measurement (nonlinearity of the produced radiation, bulk SHG and transmission coefficient) for which a specific setup is needed. We employed a Ti:Sapphire laser, with output at λ=795 nm and pulse duration τ=120 fs. This pulsed light induces the second harmonic generation in KNS.

In this chapter, we will describe the devices used and we will discuss their role in experimental setup.

2.1 **Experimental set-up**

The experimental setup is designed to study the second harmonic generation (SHG) produced by the KNS glasses. The first target was to determine if the KNS glasses could be really considered as SH converters. Then this signal was compared with the SH produced by a BBO crystal, both in phase-matching and out of phase-matching.

In figure 2.1, we show the experimental setup. The laser light, after the

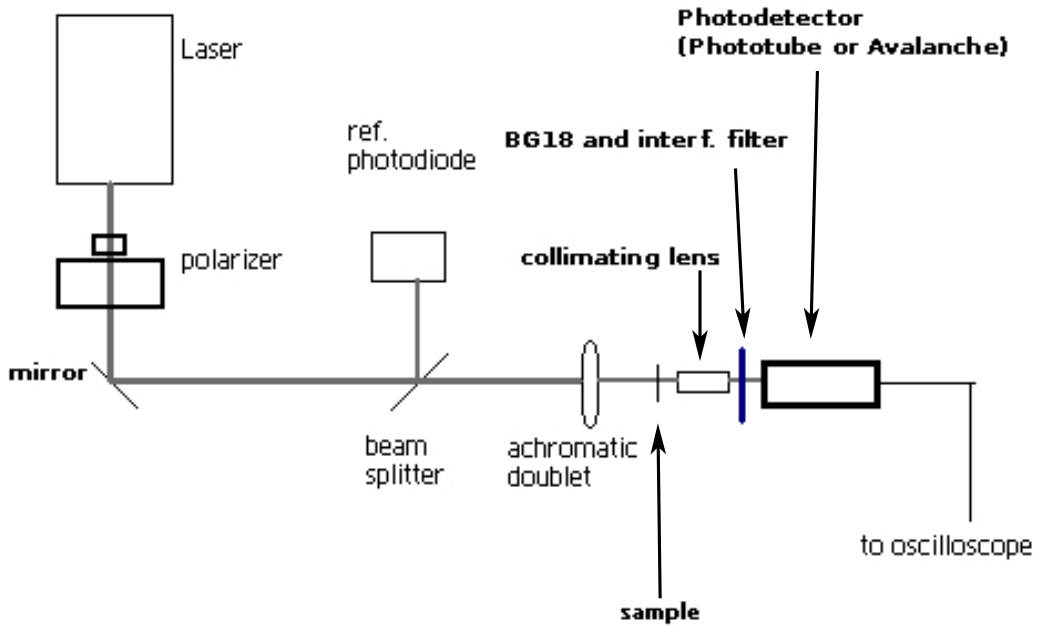

Figure 2.1: Basic setup

half-wave plate, is divided by the beam splitter that is oriented at a 45° with respect to the laser beam. The reflected beam has the 4% of the intensity of incident light. The reflected beam is recorded by a photodiode, which gives a signal proportional to the incoming power. The laser light is attenuated before the photodiode by a diffusion filter, in order to keep the device in a linear response regime and avoid saturation.

The beam transmitted by the beam-splitter is focused by the achromatic doublet on the sample, which is a 5x5x1mm sized parallelepiped. The sample is held by a support that is mounted on a system of translators, that allow

to move the sample:

1. along the z direction (the laser beam propagation direction, i.e. we move the sample in such a way that the focus can explore the sample bulk).

2. in the plane perpendicular to z direction (i.e we can move the sample in such a way that the focus can explore the area of the sample).

After the sample, the fundamental radiation and the SH travel together. They are collected by a 20x microscope objective positioned at about 1mm from the sample. The fundamental is stopped by a BG18 blue filter and the second harmonic is collected by the phototube with a bandpass filter @400 nm.

The phototube saturation is avoided by attenuating the incoming radiation trough neutral filters.

However, the SH of the phase matched BBO, was too intense and so we had to change the detector, using the avalanche photodiode.

We've performed 3 kinds of measurements: nonlinearity of the emitted radiation, bulk SHG and transmission. The primary operation was the alignment of all the setup, in particular of the achromatic doublet and of the microscope with the phototube.

Nonlinearity After positioning the sample in the focus of lens, we have changed the intensity of incoming radiation with the half-wave plate and measured SHG. This process was identically repeated for all the five samples and for the BBO out of phase-matching. Our goal was to obtain a graph showing the nonlinear behavior of KNS.

Bulk SHG It was important to determine if the SHG was due to a bulk or a surface process. We exploited the fact that the SHG is larger in the focus, because of the larger intensity. After maximizing the intensity of laser beam, we "explored" the bulk of the sample, moving the focus in the z direction. We obtained a spatial map of bulk SHG of KNS.

Transmission A slightly different setup is needed to perform the transmission coefficient measurement of KNS at 400 nm. The 400 nm radiation is externally produced by a phase-matched BBO and then was sent across the sample. Through an avalanche photodiode detector we measured the light transmitted by KNS glasses. Then we have recorded the light without the sample, deriving the KNS transmission coefficient.

2.2 Laser system

The Laser-system used is made by two main elements: a diode-pumped laser (Coherent Verdi V10) and a Ti:Sapphire oscillator (Mira Coherent 900). The laser, who acts as the optical pump of the oscillator, emits a green radiation @532 nm and has a maximum CW power of 10 W.

The oscillator, whose optical active element is a Titanium-Sapphire crystal pumped by Verdi, emits 120 fs pulses, with a repetition rate of 76MHz. The output pulses have frequency tunable in the 700-1100 nm range. The wavelength we used was 795nm and the maximum output mean power obtained was 1.8 W.

The output beam has gaussian spatial profile. We are interested to know the size of the spot, performing a knife-edge optical measurement. It consists in "slicing" the laser light with a metallic slab and measure the transmitted

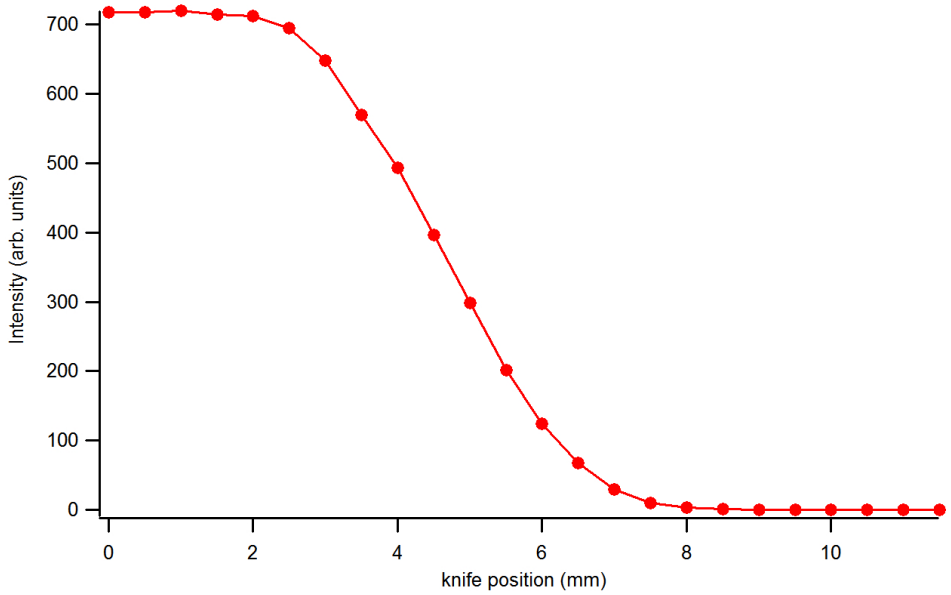

Figure 2.2: Beam profile

intensity. This is made moving the slab perpendicularly the beam.

We register the position of the slab (which is moved by a translator) and the light transmitted by the slab, using a photodiode. In such a way, we built the spatial beam profile (figure 2.2).

It is more interesting the graph showing the derivative of the knife-edge profile vs the knife position (figure 2.3). The obtained values can be fit with a gaussian function whose FWHM is the width of our laser spot. In this case we obtain the value $D = 3.3 \pm 0.5\ mm$. This element will be useful when we have to study the propagation of the laser gaussian beam throughout a focalizing lens.

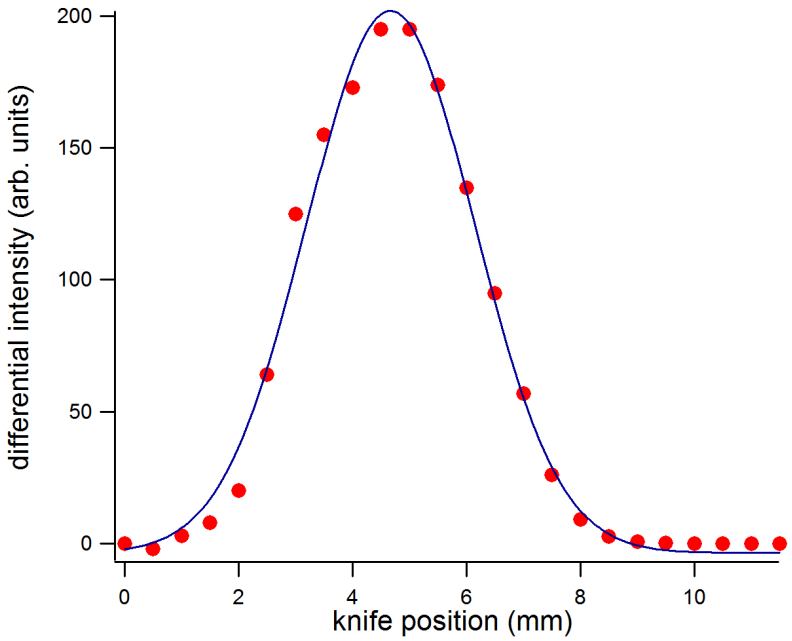

Figure 2.3: Beam profile fit with gaussian function

2.3 **Photodiode**

The Thorlabs DET210 photodiode was employed. This type of detector is a Silicon PIN photodiode, with a little (∅=1.0mm) active area, i.e. the zone of detector who interacts with the radiation. The fast response time it is suitable for detecting pulses with an high repetition rate.

In the detector, a 12V bias battery inversely polarizes the junction increasing the response time with respect to the case of unbiased diode (photoconduction regime).

The response curve of the photodiode (figure 2.5) has the maximum response at 800 nm (that is our work wavelength), where the responsivity is about 0.4 A/W. The damage threshold is 100 mW in continuous wave (CW) and 0.5 J/cm^2 for 10ns pulsed wave. The linearity limit is 1mW in CW.

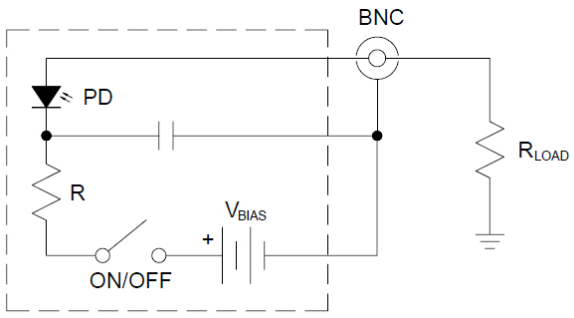

Figure 2.4: Scheme of Thorlabs DET210 photodiode

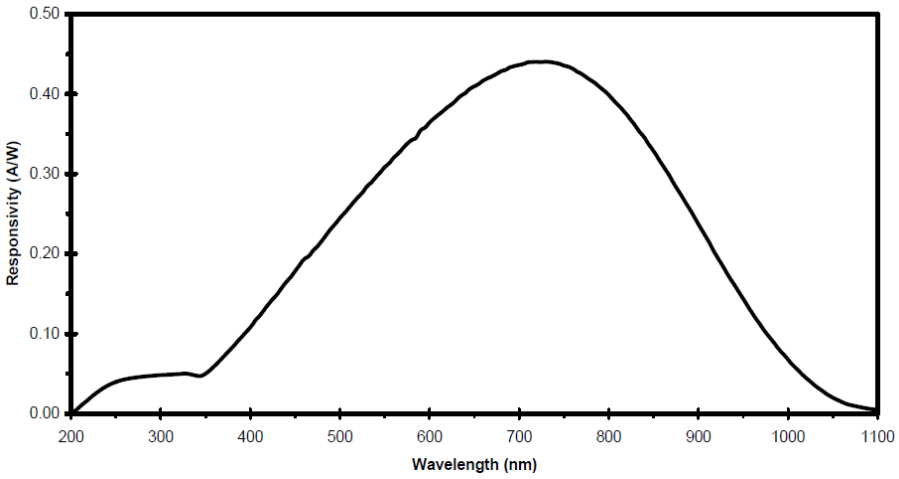

Figure 2.5: DET210 photodiode spectral response

The detector is wired by a BNC coaxial cable to the oscilloscope. The input impedance of oscilloscope is set on $1M\Omega$.

The photodiode detector can be visualized as a RC circuit, with a relaxation time $\tau = RC$. The increase of τ means that we are making an integration of the signal over a larger time window. Hence we will measure a mean signal that is an average of peaked signal corresponding to the current

pulse generated in measurement.

The detection device includes a diffusion filter to attenuate the laser light. In such a way we avoid the saturation and the device works in his linear range.

2.4 **Avalanche photodiode**

In order to acquire a signal too low to be detected by a normal photodiode but too high for a phototube, we use an avalanche photodiode.

An avalanche photodiode is a p-n junction with a high doping level. When it is inversely polarized, the carriers created by illumination are accelerated by the electric field. The carriers acquire kinetic energy to create by collision new electron-hole pairs, trough electron-electron collision. This process happens several times, so that the absorption of one photon generates several carriers. Because the carriers are subjected to a strong acceleration due to electric field, we can obtain very short transit times. This class of photodiode is used to detect weak and short signal, below the detection threshold of a normal photodiode.

We used the Menlosystems APD210, that has a 400nm-1100nm spectral range (figure 2.6), to detect the SH generated by a phase-matched BBO nonlinear crystal. The active area has very small dimensions ($\varnothing = 0.5mm$). The detector was used at its maximum gain ($2.5 \cdot 10^5$ V/W), because of the low intensity of the incident signal. The avalanche was connected to the oscilloscope with a BNC coaxial cable.

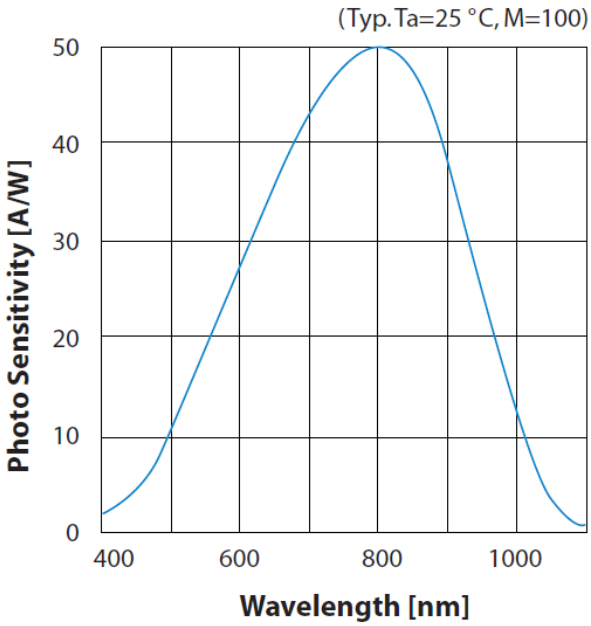

Figure 2.6: Avalanche APD210 spectral response

2.5 **Photomultiplier**

This kind of detector is characterized by the high sensitivity, allowing to detect single photons.

It consist of a photocathode, a chain of dynodes and an anode that works as collector of electrons (figure 2.7). The light reaches the photocathode, where electrons are emitted, due to photoelectric effect. The dynodes chain accelerates the electrons which finally arrive at the anode, generating an amplified current pulse.

The photocathode is composed by a low-work-function material (typically multi-alkali compounds or semiconductors, such as GaAs or InGaAs).

We define the quantum efficiency η as the number of electrons emitted

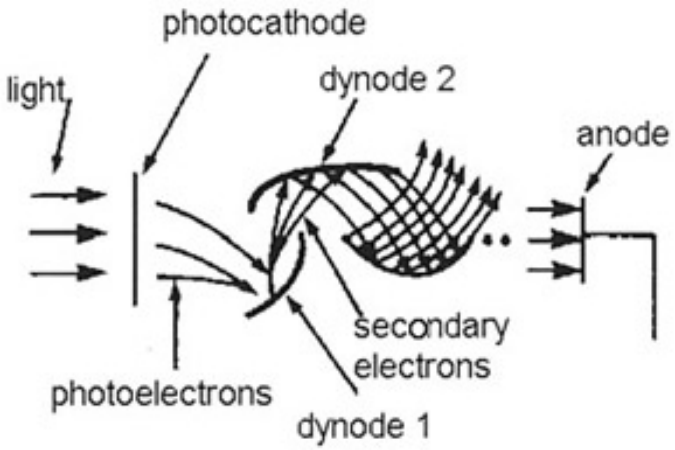

Figure 2.7: Photomultiplier scheme

per incident photon:

$$\eta = \frac{n_{el}}{n_{phot}}.$$

A typical parameter is also the responsivity $\mathcal{R}$, that is the generated current divided by the power of incident beam:

$$\mathcal{R} := \frac{I}{P} = \frac{e\, n_e}{\tau} \frac{\tau}{h\nu\, n_{ph}} = \frac{e\eta}{h\nu} = \frac{e\, \eta\, \lambda}{hc},$$

where λ is the wavelength of incoming radiation, τ the pulse duration of the radiation and e the electron charge.

The dynodes are composed by CsSb, a material with a very high secondary electron emission coefficient. Thus when an electron from the photocathode reaches the first dynode, several electrons are emitted from it. These secondary electrons kick the second dynode where an analogue process takes place.

The amplification factor is given by the coefficient of secondary electrons emission δ (i.e. number of electron emitted by dynodes per incident electron).

Therefore the gain of photomultiplier depends on the number n of dynodes and is given by $G = \delta^n$. So that, the responsivity for a photomultiplier is

$$\mathcal{R}_{PMT} = \frac{e \cdot \eta \cdot \lambda}{hc} G$$

The system is in vacuum (10^{-4} bar) in order to increase the free mean path of the electrons. The tube is assembled on a socket that provides the voltage. Finally, the signal output is amplified by an operational amplifier. We used an Hamamatsu R7518 with a C6270 socket supply. We used this device to detect the intensity of SH (λ=400nm), where the spectral response of detector is maximum. (figure 2.8)

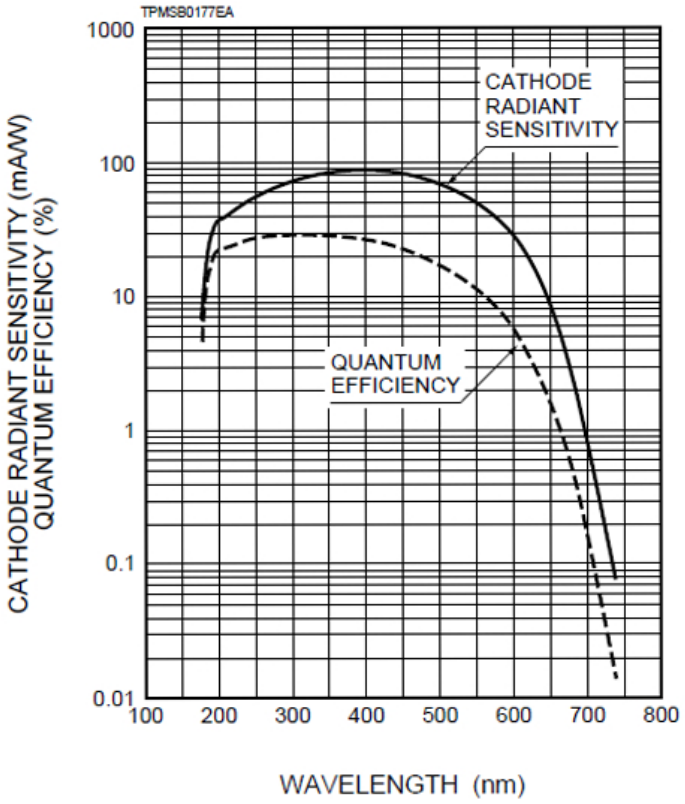

Figure 2.8: R7518 spectral response

The device is connected to a digital oscilloscope by a BNC cable. We

acquire the current generated by the tube as a voltage difference, by closing circuit on a 1 $M\Omega$ resistance. To decrease the noise, we acquire the average signal over a temporal window.

It is important work in a dark environment, because the laboratory light could damage the dynodes in a permanent way.

An interferometric filter at 400 nm is inserted on the window of the photocathode. In this way, we detect only light with frequency centered around that value.

We however noted that the measurement was affected UV radiation generated by some control displays. Thus we was careful to cover this UV sources.

2.6 **Power Meter**

The photomultiplier tube gives us a voltage signal, related to the pulse current produced by the photons for photoelectric effect. Unfortunately it is difficult to directly relate the signal to the incident power.

In order to determine the conversion scale, we used a power meter. It's based on the principle that the optical power is converted to heating power in some absorber structure, and the resulting temperature rise is measured, e.g. with a thermopile. The Ophir 3A-SH gives a mean value of the incoming power of the laser radiation.

The energy content of each pulse of the incident radiation is given by:

$$E_p = (\text{Power meter signal in W})/R_r,$$

where R_r is the repetition rate of the laser. The peak intensity is given as:

$$I_p = \frac{E_p}{A\tau} \tag{2.1}$$

where τ is the duration of a single pulse and A the area on the sample. In our case, we evaluated the area of the beam in the focus of an achromatic doublet.

For example, if we measure with power meter a signal of 76 mW, for our laser we have a pulse energy:

$$E_p = \frac{\text{PM signal [mW]}}{R_r} = \frac{76mW}{76MHz} = 1nJ.$$

2.7 Filters

The optical filter are used to attenuate the incident signal (NG5 and NG11 filters) or stop a component with a specific wavelength (BG18 filter).

The NG11 and NG5 filters are neutral glass filters that attenuate the incoming radiation. They are designed to cover a spectral range from 400 to 1100 nm. The NG5 transmission coefficient at 800 nm is 0.5, the NG11 transmission coefficient for the same wavelength is 0.68.

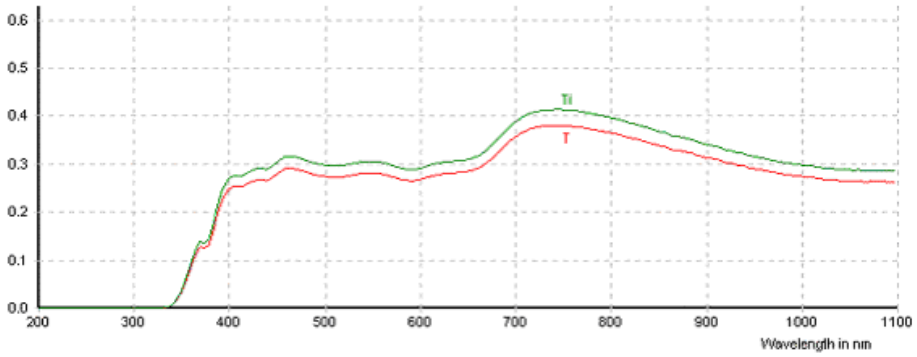

Figure 2.9: NG5 transmission coefficient (d=1mm)

The BG18 filter is a blue bandpass filter, that is designed to block the red component of the radiation. The transmission coefficient for a 800 nm

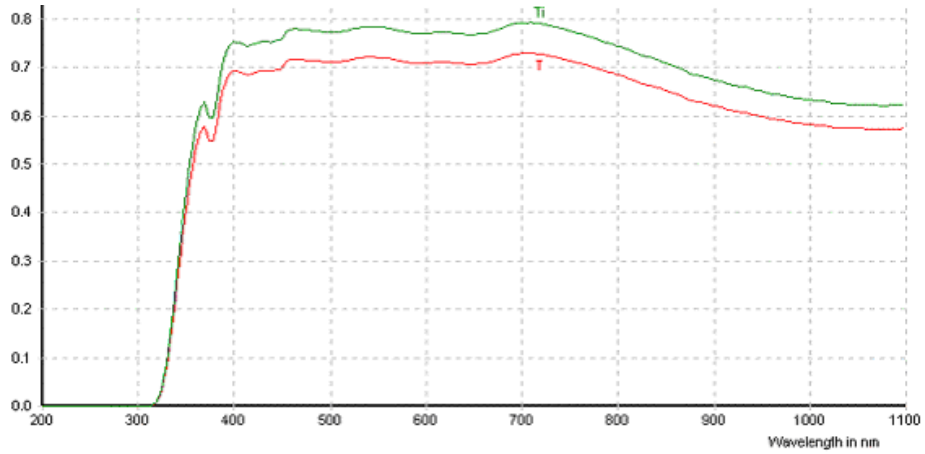

Figure 2.10: NG11 transmission coefficient (d=1mm)

radiation is $7.6{\cdot}10^{-5}$, whereas it is $6.8{\cdot}10^{-1}$ for a 400 nm radiation (our SH). For this reason, we will use the BG18 in order to separate the fundamental to the second harmonic.

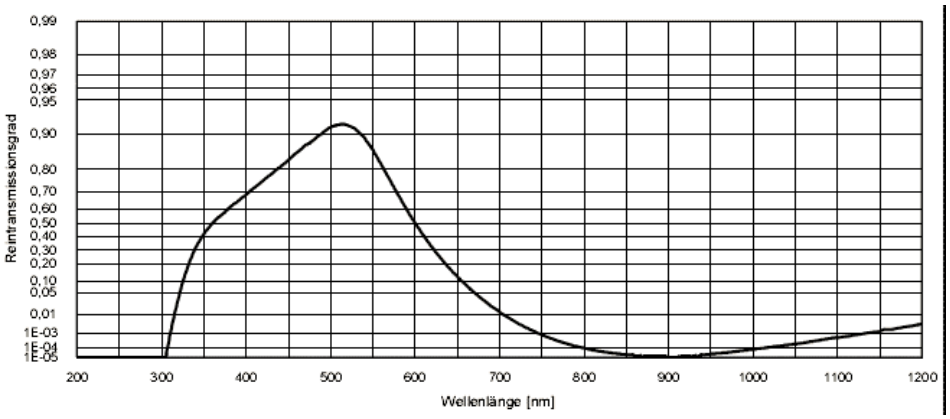

Figure 2.11: BG18 transmission coefficient (d=1mm)

2.8 **Half-wave plate and beam-splitter**

We used a polarizer combined with an half wave plate to control the incoming radiation intensity. The polarizer is composed by two calcite prisms, separated by an air interface.

The working principle of this device is the total internal reflection. As a consequence of the birefringence of the calcite, the total reflection angle is different between the two polarization of light.

So, at the critical angle, only a polarization of incident light pass trough the polarizer. The other one is totally reflected and goes out the device through an escape port. For this reason, the device does not absorbs the energy of light in the polarizing medium, so that it is not damaged when exposed to high light intensity.

At 800 nm, the polarizer has an high extinction factor (10^{-5}). In our experiment the polarizer has a fixed angle while we rotate the half-wave plate to change the intensity of light incident on samples.

Rotating the half-wave plate, we change the polarization component of the incident light. Combining this effect with the polarizer we obtain a different out-coming intensity.

The beam splitter is a device built to work in IR optics, with ultra short pulses. It splits the incident beam in 2 rays, with a reflection coefficient of 0.3 and a transmission coefficient of 0.7. It is designed in order to preserve the pulse shape and to minimize the spatial and temporal dispersion.

2.9 **Achromatic doublet**

An IR achromatic doublet was employed to focus the 800 nm beam on the sample. This device is designed to avoid chromatic aberration effects i.e. focus length different for different wavelength. The control of these effects is crucial for femtoseconds light pulses with a quite large spectral content.

The doublet has a diameter of 25.4 mm and a focal length of 50 mm. Moreover, it is anti-reflection coated for the wavelengths from 650 to 1100 nm.

We can estimate the dimension of the focus using the propagation theory of gaussian beams. Consider the optical system in figure 2.12.

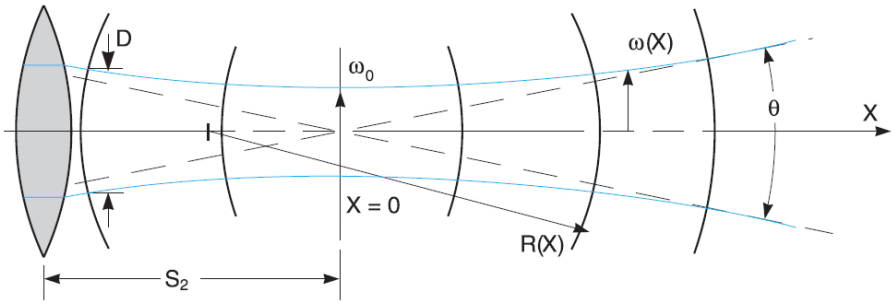

Figure 2.12: Gaussian propagation through a lens

We define the spatial range where the power decreases of the 5% with respect to the power in the focus as the Rayleigh range, given by the expression:

$$x_r = \frac{0.32\,\pi w_0^2}{\lambda},$$

where w_0 is the spot ray in the focus and λ the wavelength of the radiation, in our case the central wavelength on which the pulse is centered.

The focus depth is $2x_r$. The spot diameter in the focus is given by the

expression

$$d_0 = 2w_0 = \frac{4\lambda f}{\pi D},$$

where f is the focal length of the lens and $D = 3.3mm$ is the spot diameter before the lens, which was obtained with a knife-edge method described in 2.2.

In our case we have a focus depth $2x_r = 150 \pm 10\mu m$ and a spot diameter in the focus $d_0 = 15 \pm 3\mu m$. In order to verify these data, we repeated the knife-edge measurement, but in the focus of the lens. We obtained a spot diameter $d_0 = 9 \pm 5\mu m$, that is comparable with the estimate value.

3. Measurements

As explained in the previous chapter, we performed three kinds of measurements: nonlinearity, bulk SHG and transmittance. The results obtained allow to underline several interesting features of KNS glasses.

3.1 Nonlinearity

The first aim of our research was to show that KNS glasses behave as second harmonic generators. For this reason, after mounting the setup as in figure 2.1, we have performed for each of the five samples a non linearity measurement, i.e. the recording of the fundamental signal incident on samples and the correspondent SH signal produced.

The reference photodiode and the phototube give a voltage signal proportional respectively to the power of incoming radiation and to the power of SH radiation. The system was previously calibrated, as described in section 2.6 to convert the voltage acquired on oscilloscope to the incident power.

In this first graph (figure 3.1), we show the nonlinear behavior of the five

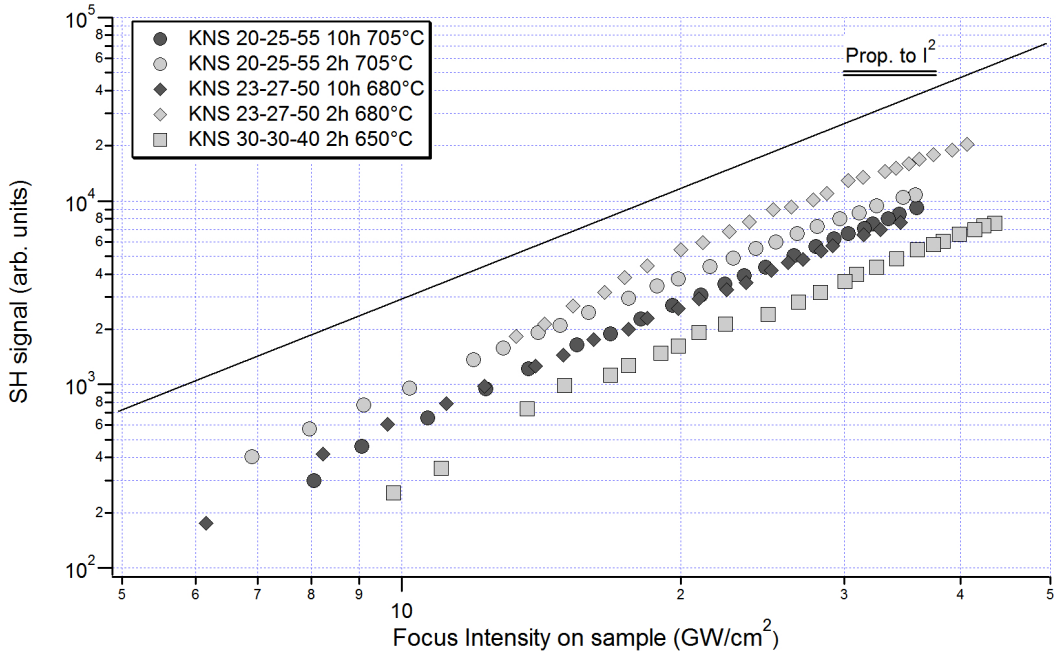

Figure 3.1: SHG in KNS glasses

samples. The graph is in a logarithmic scale. The black line represents a quadratic function.

We find out that $I(2\omega) \propto I^2(\omega)$, that is the relation that identifies the SHG process.

As you can see, all the samples produce SH signal but there are some differences among the various samples. The most intense SH signal is obtained from sample S1 (KNS 23-27-50 2h 680°C), the worst from sample S6 (KNS 30-30-40 2h 650°C).

It is meaningful to calculate the SH conversion efficiency $\mathcal{E}_{SHG}$ for KNS, i.e. the ratio between the number of SH photons generated and the number of incident photons:

$$\mathcal{E}_{\mathrm{SHG}} = \frac{\mathrm{I}(2\omega)}{\mathrm{I}(\omega)}$$

We have compared the KNS efficiency with efficiency of a nonlinear medium well-described in the literature, such as a BBO crystal. In particular we used a BBO 8.5x5x0.3 mm sized, cut at θ=46° and ϕ=0° (type I). This crystal could be employed for SHG with the Ti:Sapphire laser, considering a phase-matching angle of about 30° with respect to the optical axis.

At first we have determined the SHG conversion efficiency of the phase-matched BBO (PM-BBO) measuring the mean power of the fundamental and the mean power of the second harmonic with the powermeter. For values of incoming intensity close to 32 GW/cm^2 on the crystal, the phase-matched BBO has a second harmonic conversion efficiency of 0.002 ± 0.0004, i.e. two photons over 10^3 are converted.

As said, our aim was to determine the SHG efficiency of KNS glasses. However, the SH generated by KNS can't be directly detected by the calibrated powermeter, but only with the phototube (because of low SH intensity and mean power). In graph 3.2 we show the detection range of the devices used.

Hence, the problem was the conversion of the relative SH voltage signal, measured with the phototube from KNS, in an absolute power signal. We proceeded in the following way:

1. We measured, using the powermeter, the mean power of the input IR radiation and of the SH signal generated by the phase-matched BBO determining the SHG efficiency of the crystal. Then we measured the corresponding SH voltage signal with an avalanche photodiode. The

avalanche was employed because with SH intensity generated by the phase-matched BBO the phototube saturated, even at the maximum available attenuation from neutral filters. In such a way we derived the the conversion factor between the mean power of the SH radiation and the voltage read on the oscilloscope from the avalanche photodiode.

2. We detected, using the calibrated avalanche, the SH intensity of an out-of-phase-matching BBO, that has a lower SH conversion efficiency. Then we measured the same signal with the phototube calibrating the phototube against the avalanche photodiode. We employed suitable neutral filters, with a known attenuation coefficient, in order to avoid phototube saturation.

3. Finally, we measured the SH signal produced by KNS with the calibrated phototube.

Therefore, we measured the ratios among the SH signals produced by the three different calibrated devices, converting the voltage signal of KNS to power units and deriving the SHG efficiency. We estimate the errors on the measurement within a range of twice the values collected.

In the graph 3.2 we plot the incoming power on samples vs their second harmonic generation efficiency.

We also report the SHG from a out-of-phase-matching BBO, to underline the different efficiency. The SH efficiency of the BBO is 5-6 order of magnitude larger than the KNS one. The black lines in figure 3.2 represents a linear function.

The KNS can convert about only one photon over 10^{10}, while even the not phase matched BBO produces SH photons with an efficiency of one photon

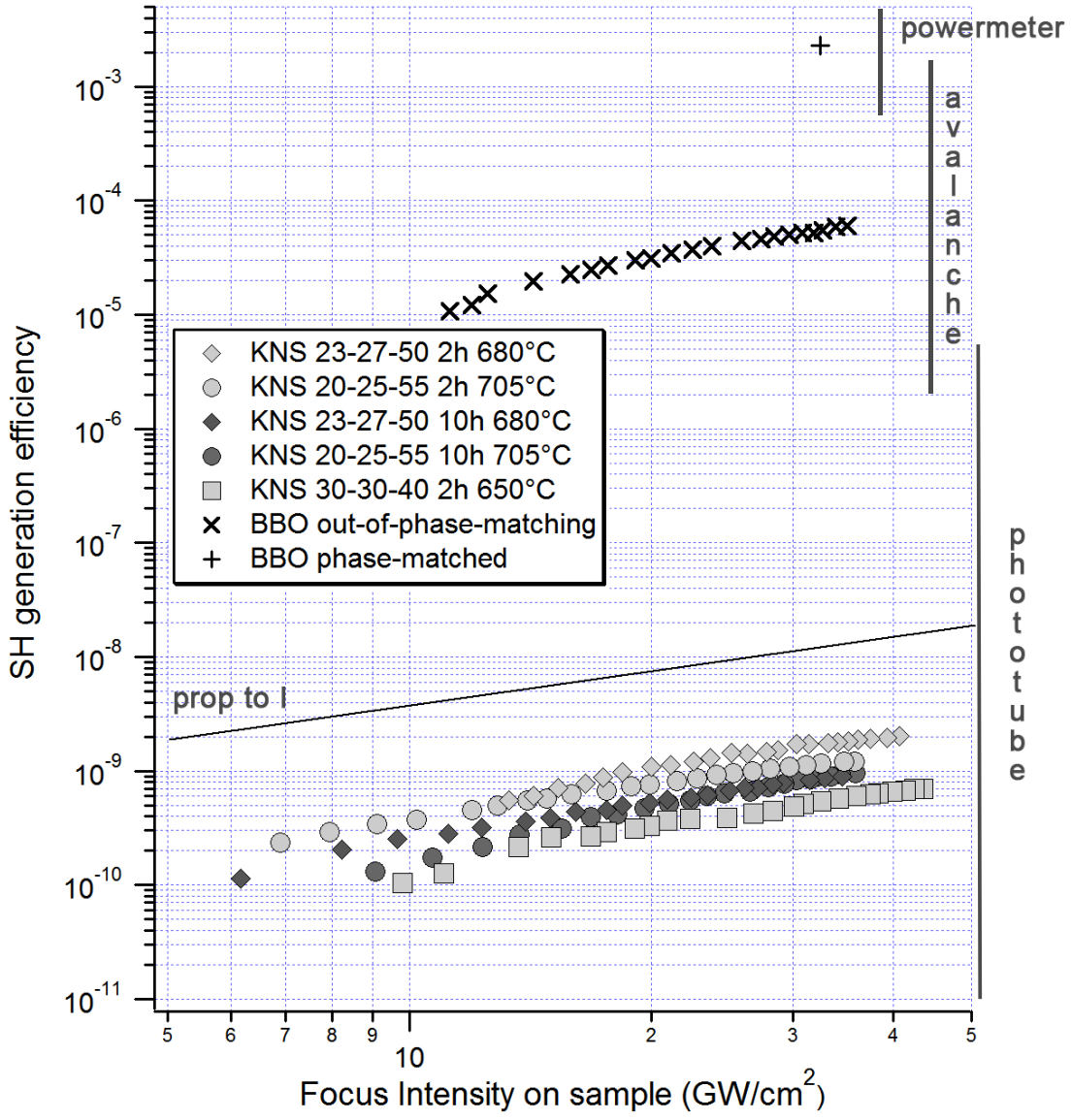

Figure 3.2: SHG efficiency in KNS glasses and BBO crystal, with detection range of the employed devices

over about 10^5.

Because the $I(2\omega) \propto I^2(\omega)$ and the efficiency is defined as $I(2\omega)/I(\omega)$,

the conversion efficiency is linear with respect to the intensity of incident radiation:

$$\mathcal{E}_{\mathrm{SHG}} = \frac{\mathrm{I}(2\omega)}{\mathrm{I}(\omega)} \propto \frac{\mathrm{I}^2(\omega)}{\mathrm{I}(\omega)} = \mathrm{I}(\omega)$$

3.2 **Bulk SHG**

The second series of measurement, was aimed to investigate the SHG origin in KNS glasses. As we explained in chapter 1, KNS glasses are polycrystalline materials, formed by nanocrystals randomly arranged in the material and surely smaller than the wavelength of the fundamental incoming radiation.

The measurement consists in moving the sample, using the translation system, in order to scan with the doublet focus, at fixed power of the incoming radiation, the bulk of the KNS, collecting with the phototube the SH signal.

In fact, the focus of lens is the point where the power is larger and consequently the SHG has its maximum efficiency. The signal we read so represents the SH generated in the focus length (in our case 150μm).

The first result is that the SH signal is almost the same in all the points of the surface of sample. This indicates that the production is homogeneous in all the material. The second consideration is that the SH is an evident bulk effects, that is the SHG process takes place in the volume of the sample.

In the graph in figure 3.3 the SH signal vs the position of focus in the sample is reported.

We have not a punctual focus, but a focus with a measurable length. For this reason, we expect a SHG bulk pattern which is convolution of a gaussian function (that represents the dimension of focus) with a step function (that represents the real thickness of the sample).

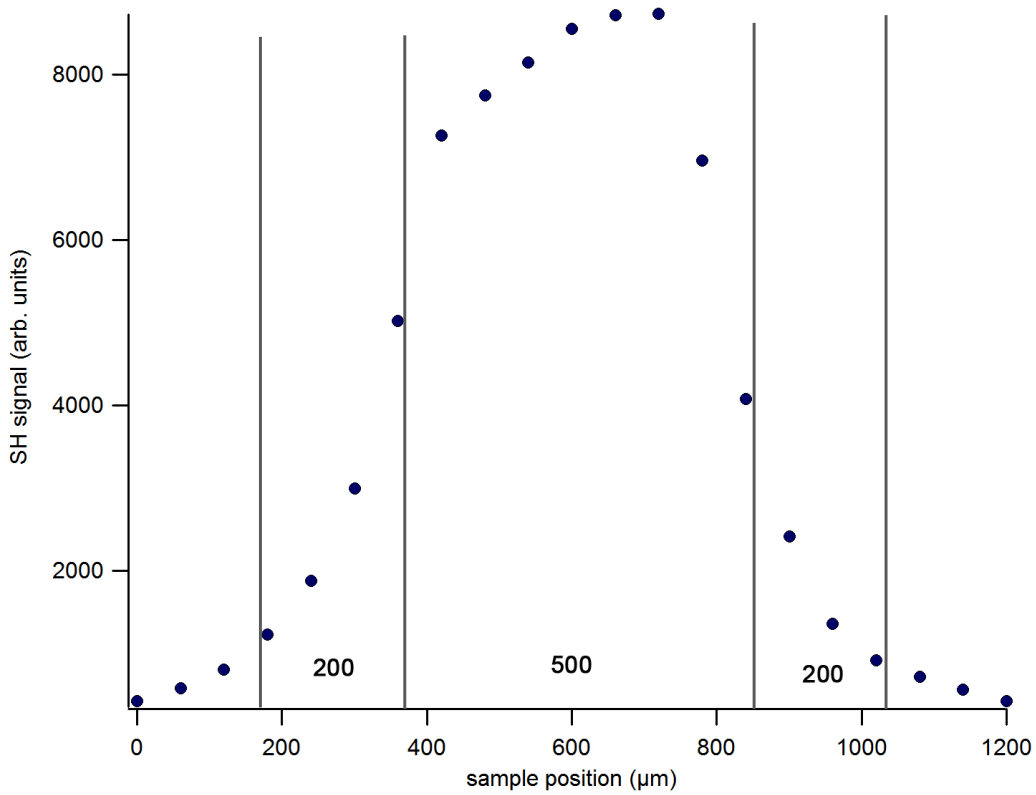

Figure 3.3: Bulk SHG in S2 sample, values in μm

We also expect that the convolution width will be comparable with the thickness of the sample (1 mm).

We have divided the graph in figure 3.3 in three regions. The central one (widht=500 μm) represents the passage of the focus totally in the bulk. The lateral ones are corresponding to the passage of focus at the surfaces. Notice also that the total width of the graph is about 800-900 μm, comparable with the thickness of sample.

We have compared the bulk SHG in the KNS glasses with the SH gener-

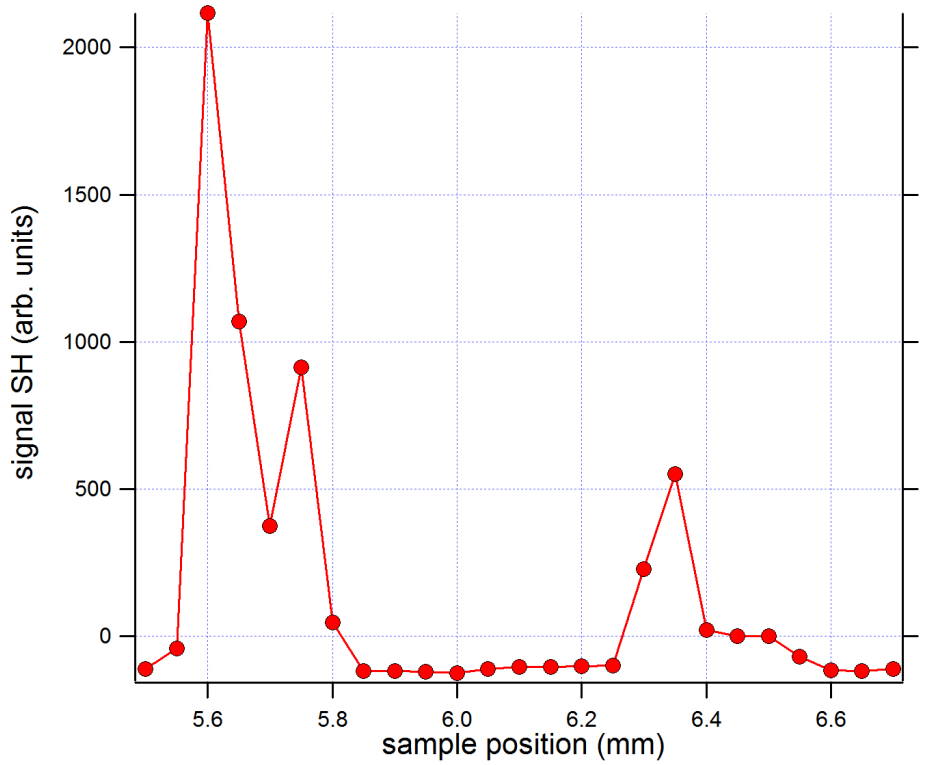

Figure 3.4: SHG bulk pattern in fused silica

ated by a fused silica slab, that is surely due to superficial effects.

The SH from surfaces is obtained with the same method employed for the measurement of bulk SHG in KNS glasses. But, on the contrary, for a surface SHG process, we would expect a double-peak pattern, where every peak represents the SHG due to the light in the doublet focus interacting with the single surface (figure 3.4).

Notice that no SH signal is produced in the bulk of fused silica. This involves that the SHG process of KNS is radically different from the SHG due to superficial effects.

3.3 Transmittance

In order to realize performing and efficient KNS converters, a high SH signal transparent glass matrix is needed, because the SH signal that is generated inside the glasses by the interaction between light and nanocrystals can be transmitted outside the material without power loss.

For these reasons, we are interested to measure the transmission coefficient of the KNS glasses. The technique employed in this case was to generate the SH at 400nm outside the KNS glass, with a phase-matched BBO. Then, we have submitted the KNS to this radiation, measuring its transmission coefficient τ with a avalanche photodiode.

Id sample	τ
S1	0.81
S2	0.82
S3	0.62

The results are that the transmission coefficients are very high, so that the glass matrix that composes the KNS is ideal for performing SH converters.

We have performed this measurement only for three samples, but we can hypothesize that the transmission coefficient is similar for all the samples, because the samples are composed and prepared in the same manner.

3.4 As-quenched samples

We've examined also the SH signal generated by crystals not submitted to the annealing process (i.e. a second thermal process that causes the crystallization of glass), described in section 1.2.

In graph we can see the conversion efficiency of these last samples compared with results obtained in section 3.1.

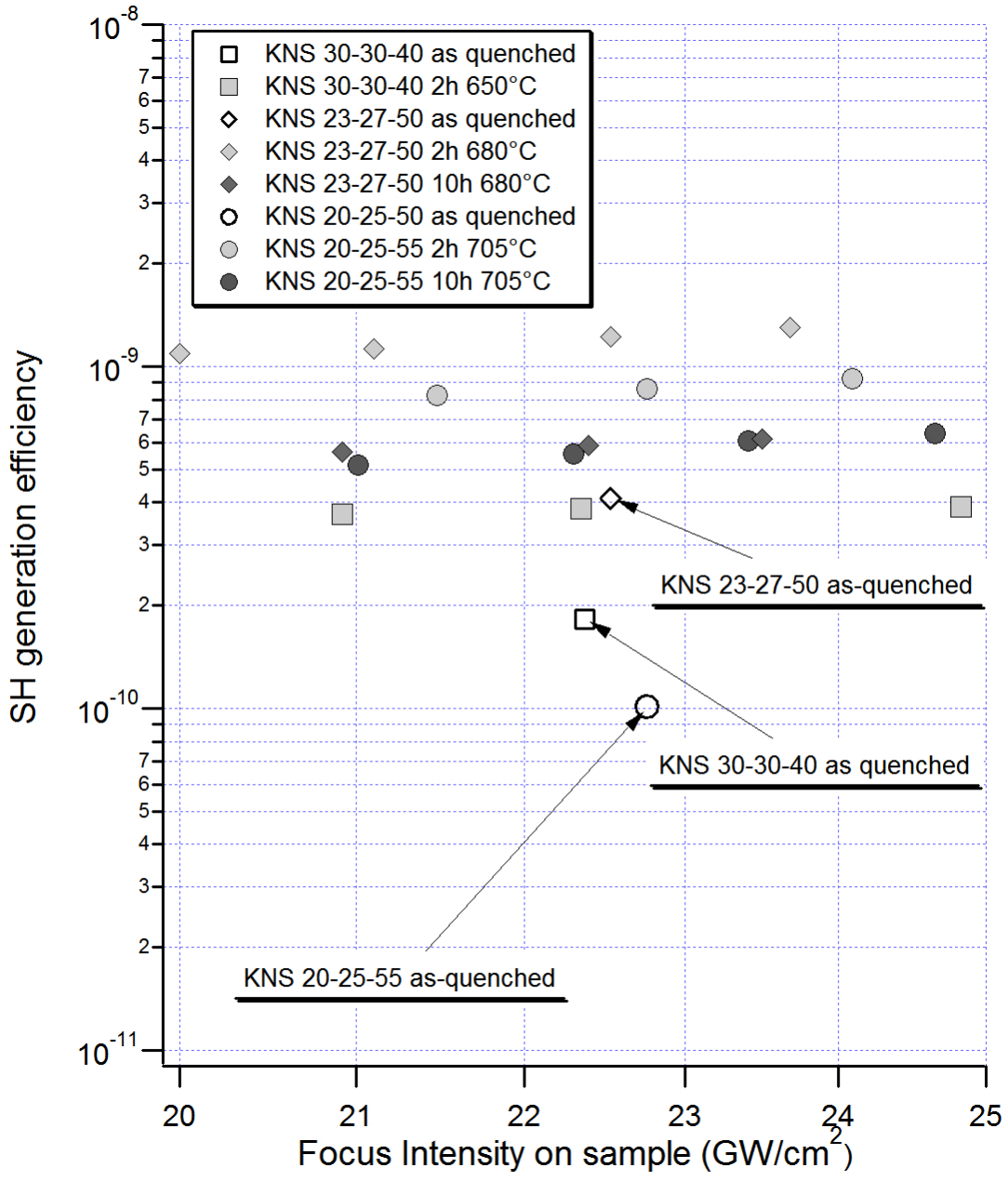

Figure 3.5: SHG in as-quenched KNS

We see that for all the kinds of sample, the annealing process improves the SHG.

Notice also that the SH signal produced by the as-quenched samples is less than the SH in samples exposed to a 2h long lasting process. The samples exposed to a 10h long process show a signal less than the 2h annealed glasses.

So, long annealing processes do not improve the SH conversion efficiency. This fact can be related to the effects induced on the growth of nanocrystals by the annealing process.

4. Conclusions

We have investigated SHG process in potassium niobium silicate ceramic glasses (KNS) and we have compared it with the SHG process in a phase-matched and out-of-phase-matching BBO crystal. The SHG signal in KNS glasses is 5 order of magnitude less than a non phase-matched BBO. However, the SHG is observed always without requiring peculiar phase-matching conditions.

We have demonstrated that the SHG is a bulk effect of the glasses, not due to superficial phenomena. but probably related to the KNS random nanocrystalline structure. At the present state, the nanocrystalline phase hasn't been yet established.

If the crystal in the glass matrix are not-centrosymmetric, surely the SHG is due to them, but if they are centrosymmetric, we have to elaborate a more complicated theory to explain the effect.

The annealing process at T_g in two cases really improves the SHG conversion efficiency even if the improvement factor is small.

At the present state, we can try to improve the SHG creating new com-

positions, changing the percent quantity of the elements. We have observed that a 2h annealing improves the SHG more than a 10h annealing.

The next step of the characterization of KNS glasses will be to discuss the role of the nanocrystals (which compose the material) in the second harmonic generation process. In particular, we are interested to investigate if the SH is generated in the bulk of nanocrystals or produced as a surface effect on the nanocrystals surfaces.

The evolution of these glasses will be the use in integrated chips or optical fibers, because they are very cheap, easy to prepare and to operate and they don't requires a careful alignment nor the high-precision engineering of microstructured samples.

Bibliography

[1] Baudrier-Raybaut M. *et al.*, Nature 432, 374-376 (2004).

[2] Skipetrov S. E., Nature 432, 285-286 (2004).

[3] Morozov E. Yu., Chirkin A. S., Quantum Electronics 34, 227-232 (2004).

[4] Fowles G. R., *Introduction to modern Optics*, New York, 1989.

[5] Hecht E., *Optics*, Reading (MA), 2002.

[6] Pernice P., Aronne A. *et al.*, J. Am. Ceram. Soc., 82 [12], 3347-52 (1999).

[7] Sigaev V.N. *et al.*, J. Non-cryst. solids, 306, 238-248 (2002).

[8] Garcia Solè J., Bausà L.E., Jaque D., *An introduction to the Optical Spectroscopy of inorganic Solids*, New York, 2005.

[9] Saleh B.E.A., Teich M.C., *Fundamental of Photonics*, New York, 1991.

[10] Franken P.A., Hill A.E. *et al.*, Physical Review Letters, 4, vol. 7 (1961).

[11] Pernice P. *et al.*, J. Non-cryst. solids, 275, 216-224, (2000).

[12] Kim H.G. *et al.*, J. Non-cryst. solids, 208, 303-307 (1996).

[13] E.M. Vogel, M.J. Weber, D.M. Krol, Phys. Chem. Glasses 32 (1991) 231.

[14] W. Nie, Adv. Mater. 5 (1993) 520.

[15] V. Nazabal, E. Fargin, J.J. Videau, G. Le Flem, A. Le Calvez, S. Montant, E. Freysz, A. Ducasse, M. Couzi, J. Solid State Chem. 133 (1997) 529.

[16] Yu-Hua Kao, Yi Hu, Haixing Zheng, J.D. Mackenzie, K. Perry, G. Bourhill, J.W. Perry, J. Non-Cryst. Solids 167 (1994) 247.

[17] K. Shioya, T. Komatsu, Hyun Gyu Kim, R. Sato, K. Matusita, J. Non-Cryst. Solids 189 (1995) 16.

[18] Yariv A., *Quantum Electronics*, New York, 1989.